

# The Optimization of Switching Scheme in Multi-Layer Phase-Modulated Surface and Its Influence on Scattering Properties

Yi Fu and Tao Hong\*

**Abstract**—To improve absorbing properties of phase-modulated surface (PMS), the multi-active-layer PMS composed of multiple active frequency-selective surface (AFSS) layers and one background plane is theoretically studied using time-modulation theory in this paper. The optimization of PMS's switching scheme using differential evolution (DE) algorithm is also proposed for minimizing scattering echo energy at the incident frequency. We provide analytical formulation for the scattering problem and obtain the angular scattering pattern of PMS after optimization. Simulation results indicate that the optimized switching scheme is beneficial for reducing the spatial coverage of scattering echo at incident frequency. This coverage can be further confined by the increasing number of active layers in PMS. Furthermore, it is shown that floor effect appears when the number of active layers reaches a certain value, which limits the PMS structure conversely.

## 1. INTRODUCTION

The principle of radar absorbing material (RAM) is to reduce radar cross section (RCS) of the target. Conventional (passive) RAM operates either by phase cancellation or by absorbing incident electromagnetic energy and converting it into heat. Because electromagnetic environment becomes more and more complex, conventional RAM with fixed working frequency and bandwidth is unable to deal with the emergency. To overcome this problem, the active RAM emerges and becomes an advanced research hotspot.

Active frequency-selective surface (AFSS) is used to design active RAM due to its variable effect on electromagnetic field behavior. The scattering characteristics of AFSS can be adjusted flexibly by regulating the current or voltage applied to it. This property makes it applied in the design of radome [1], implementation of beam control [2] and suppression of radio frequency interference (RFI) [3], etc. In [4], Tennant and Chambers from the UK's University of Sheffield designed phase-modulated surface (PMS), which is composed of single AFSS layer and one metal background plane. In [5–7], the transmission line theory was used to analyze the PMS, and results demonstrated that the regulation in switching scheme of AFSS layer would lead to the variation in scattering characteristic of PMS. In [8, 9], the authors used finite-difference time-domain (FDTD) and time-modulation theory to analyze PMS respectively. Besides in accord with the results based on conventional transmission line theory, time-modulation theory allows finite-sized PMS to be analyzed. In [10, 11], an 'array' polynomial approach was conducted to predict the positions of the reflectivity nulls for PMS, and the results indicated that the range of reflectivity null was expanded by regulating the switching scheme of PMS. In [12], the authors designed an ultra-thin broadband AFSS absorber with a stretching transformation (ST) pattern for use in the ultrahigh-frequency (UHF) band. Results indicated that the absorbing bandwidth of absorber was expanded by adjusting the unit cell pattern of AFSS. Therefore, the unit cell pattern

---

*Received 29 December 2015, Accepted 29 February 2016, Scheduled 9 March 2016*

\* Corresponding author: Tao Hong (hongt@njupt.edu.cn).

The authors are with the College of Telecommunications and Information Engineering, Nanjing University of Posts and Telecommunications, Nanjing 210003, China.

and the switching scheme of AFSS are both associated with the absorbing performance of PMS. Due to its unique electromagnetic property, PMS was used to reduce the RCS of spiral patch antenna [13], generated SSB or QPSK modulation signal [14, 15] and lowered the power spectral density (PSD) of echo scattered from PMS [16]. Besides PMS, several new techniques or materials have been proposed for the design of active RAM in the past few years, e.g., graphene-enabled electrically switchable radar-absorbing surfaces relying on electrostatic tuning of the charge density on an atomically thin graphene electrode [17], inkjet printing technology in which the volume ratio of an aqueous vehicle and nano-silver (Ag) ink mixture is adjusted to change the surface resistances [18] and semiconductor nanoparticles whose particle size and hydrogenation condition are connected with its electromagnetic characteristic [19], etc.

In this paper, PMS composed of multiple AFSS layers and one background plane is considered, which is called here multi-active-layer PMS. An analytical formulation is provided for a scattering problem involving a plane wave normal incident on the PMS. The method for the analysis is based on time-modulation theory which enables finite-sized PMS to be analyzed. The optimization of PMS's switching scheme using differential evolution (DE) algorithm is proposed for minimizing scattering echo energy at the incident frequency. The angular scattering pattern of PMS is obtained for the comparison with previous work. The originalities of this paper are as follows:

i) Time-modulation theory is used to analyze the scattering properties of single-active-layer PMS in [9], and we find the fundamental scattering energy of PMS is residue due to its finite size. The multi-active-layer PMS studied here successfully reduces this energy to a lower level and helps avoid being detected by radar as a result; ii) Enlarging the size of PMS directly is a method to reduce the fundamental scattering energy of PMS; however, we obtain this reduction by optimizing the switching scheme of PMS, and the differential evolution (DE) algorithm is used for the optimization. Results indicate that the method proposed in this paper has a better performance in improving the absorbing performance than enlarging the size of PMS under the same construction complexity; iii) An expanded absorbing bandwidth is obtained in papers [10–12]. However, we do not expand the absorbing bandwidth of PMS in infrequency domain but reduce the spatial coverage of scattering echo energy, which actually expands the absorbing “bandwidth” at spatial angle; iv) By studying PMS with different numbers of active layers, we summarize the variation tendency of the fundamental scattering energy of PMS and find that the floor effect appears during the variation process, which means that the number of layers in PMS should be confined; therefore, the research in this paper is beneficial for finding a balance point in improving the absorbing performance of PMS and reducing its construction complexity at the same time.

Our paper is organized as follows. An analytical formulation is provided for the scattering problem involving a plane wave normal incident on the PMS in Section 2. According to the analytical formulation, in Section 3, the PMS composed of two active layers is studied as an example, and a solution of its switching scheme is obtained by DE algorithm. Then our approach is illustrated by angular scattering patterns obtained from numerical simulations in Section 4. Furthermore, we study the PMS with more active layers and give a summary on the scattering properties of PMS in Section 5. Finally, this paper is summarized with conclusions in Section 6 and the acknowledgment in Section 7.

## 2. BASIC ANALYSIS

In this section, an analytical formulation is provided for the scattering problem involving a multi-active-layer PMS by assuming that the PMS is illuminated at normal incidence by a monochromatic uniform plane wave. The structure of multi-active-layer PMS is shown in Fig. 1 where from layer 1 to layer  $L$  are all AFSS. The black patches represent bow-tie AFSS elements loaded by PIN diodes at their center, and the bottom is perfect electric conductor (PEC) background plane. These  $(L + 1)$  layers are separated by  $L$  low-loss dielectric spacers with the same thickness  $s$ . Because the scattering characteristics of AFSS are controlled by the applied control voltage, we make AFSS layer scatter weak when not excited and a ‘strong’ scatterer when energized by a suitable voltage. As a result, the incident wave may be scattered by different layers according to the specific excitation mode. The periodic rectangular pulse is used for the excitation, which is called switching waveforms in this paper.

Figure 2 shows the model of multi-active-layer PMS according to time-modulation theory, where

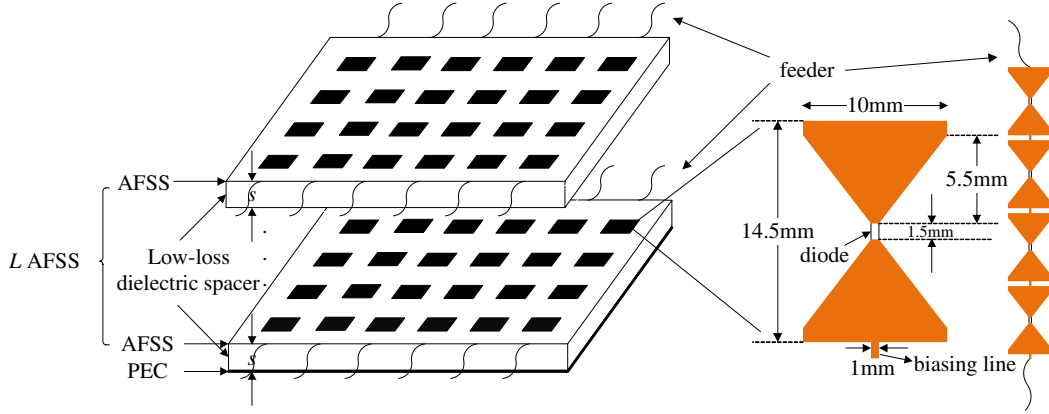


Figure 1. PMS consists of  $L$  AFSS layers and one background plane.

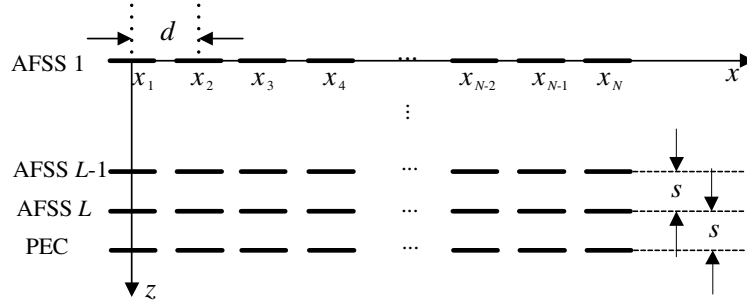


Figure 2. Equivalent model of multi-active-layer PMS based on time-modulation theory.

PMS is equivalent to  $(L + 1)$   $N$ -elements linear arrays separated by vertical distance  $s$ , and the elements in each array are located at positions given by  $x_i, i = 1, 2, 3 \dots N$ . The reason for using linear array is that the AFSS elements in one column are connected with each other.

Consider that all elements are excited with the same switching period  $T_p$ . The element status is defined “on” when it acts as a “strong” scatterer and “off” when it acts as a “weak” scatterer.  $\tau_{ki}^{on}$  and  $\tau_{ki}^{off}$  represent the switching “on” and “off” times, respectively, where  $\tau_{ki}^{on} < \tau_{ki}^{off} < T_p$ ,  $k = 1, 2, 3 \dots (L + 1)$  is the layer sequence number, and  $i = 1, 2 \dots N$  represents the element sequence

number in the array  $k$  and  $T_p = \sum_{k=1}^{L+1} (\tau_{ki}^{off} - \tau_{ki}^{on})$ . Consider that multi-active-layer PMS is normal illuminated by a uniform plane wave at frequency  $f_0$ . When the incident wave is scattered by array  $k$ , the time-domain waveform of echo in the far field at angle  $\theta$  can be expressed as:

$$f_k(\theta, t) = E(\theta) \cdot \sum_{i=1}^N U_{ki}(t) \cdot e^{j\alpha_i} \quad (1)$$

$$U_{ki}(t) = \begin{cases} 1, & nT_p + \tau_{ai} < t < nT_p + \tau_{bi} \\ 0, & \text{else} \end{cases} \quad (2)$$

where  $\theta$  is the angle between the scattering direction and the normal,  $E(\theta)$  the scattering pattern of each element,  $\alpha_{ki} = \omega_0 t + \beta[x_i \sin \theta + (k - 1) \cdot s(1 + \cos \theta)]$  the relative phase of the element  $i$  in array  $k$ ,  $U_{ki}(t)$  the switching waveform, in which the element acts as a strong scatterer when  $U_{ki}(t) = 1$  and a weak scatterer when  $U_{ki}(t) = 0$ . Since the periodical switching produces harmonics at the switching period  $T_p$ , the Fourier series form of Eq. (1) is:

$$f_k(\theta, t) = \sum_{m=-\infty}^{m=+\infty} c_m e^{j2\pi m f_p t} \quad (3)$$

$$c_m = \sum_{i=1}^N E(\theta) a_{mi} e^{j\alpha_i} \quad (4)$$

$$a_{mi} = \frac{1}{T_p} \int_0^{T_p} U_{1i}(t) e^{j2\pi m f_p t} dt \quad (5)$$

where  $f_p = 1/T_p$  is the switching frequency. We divide Eq. (3) into fundamental frequency and  $m$ -harmonic ( $m > 0$ ):

$$f_k(\theta, t) = \begin{cases} \sum_{i=1}^N E(\theta) e^{j\beta[x_i \sin \theta + (k-1) \cdot s(1+\cos \theta)]} \cdot \frac{\tau_{ki}^{off} - \tau_{ki}^{on}}{T_p} \cdot e^{j2\pi f_0 t}, & m = 0 \\ \sum_{i=1}^N E(\theta) e^{j\beta[x_i \sin \theta + (k-1) \cdot s(1+\cos \theta)]} \cdot \frac{j}{2\pi m} \cdot \left( e^{-j2\pi m \frac{\tau_{ki}^{off}}{T_p}} - e^{-j2\pi m \frac{\tau_{ki}^{on}}{T_p}} \right) \\ \cdot e^{j2\pi(f_0 + m f_p)t}, & m = 1, 2, 3 \dots \end{cases} \quad (6)$$

When all  $(L+1)$  layers are considered in the period  $T_p$ , the echo time-domain waveform in the far field at angle  $\theta$  is described as Eq. (7), which is used to explain the angular scattering pattern of PMS.

$$f(\theta, t) = \sum_{k=1}^{L+1} f_k(\theta, t) \quad (7)$$

From Eq. (7), the angular scattering pattern is associated with layer thickness  $s$ , layer number  $L$ , element number  $N$  in each array, the scattering pattern of each element  $E(\theta)$ , and the switching times  $\tau_{ki}^{on}$  and  $\tau_{ki}^{off}$ . In order to reduce the residual fundamental scattering energy of single-active-layer PMS in [9], increasing the value of  $L$  is a method. However, it is a problem to search the optimal switching scheme to minimize the fundamental scattering energy of multi-active-layer PMS. Therefore, we optimize the switching scheme of multi-active-layer PMS in the next section.

### 3. PARAMETER OPTIMIZATION

A PMS composed of two AFSS layers and one background plane is considered as an example in this section. Assume that the PMS is normal illuminated by uniform plane wave at frequency  $f_0 = 10$  GHz. The layer thickness  $s = \lambda_0/4 = 7.5$  mm, and each array contains 16 elements separated by horizontal distance  $d = \lambda_0/2 = 15$  mm. All elements have the same omnidirectional radiation pattern  $E(\theta) = 1$ .

According to the general characteristics of RAM, we expect that no energy is scattered back at the incident direction and at frequency  $f_0$ , which is described as:

$$f(0, t)_{m=0} = 0 \quad (8)$$

Transforming it to Eq. (9):

$$\sum_{i=1}^{16} \frac{\tau_{1i}^{off} - \tau_{1i}^{on}}{T_p} + \sum_{i=1}^{16} \frac{\tau_{2i}^{off} - \tau_{2i}^{on}}{T_p} \cdot e^{j\pi} + \sum_{i=1}^{16} \frac{\tau_{3i}^{off} - \tau_{3i}^{on}}{T_p} \cdot e^{j2\pi} = 0 \quad (9)$$

We define  $\Gamma_{ki} = \frac{\tau_{ki}^{off} - \tau_{ki}^{on}}{T_p}$  as duty ratio of switching waveform, where  $\Gamma_{1i} + \Gamma_{2i} + \Gamma_{3i} = 1$ . Then we simplify Eq. (9) as:

$$\sum_i^{16} \Gamma_{1i} + \sum_i^{16} \Gamma_{3i} = \sum_i^{16} \Gamma_{2i} = 8, \quad i = 1, 2, 3 \dots 16 \quad (10)$$

It is noted that the condition in Eq. (10) only produces zero backscattering at the incident direction and at frequency  $f_0$ , which means that the fundamental scattering energy is residual at other directions. If radar receivers exist randomly at the angle  $\theta \in [-90^\circ, 90^\circ]$  away from the incident direction, the residual energy is harmful to target stealth. To overcome this problem. The optimization of  $\Gamma_{1i}$ ,  $\Gamma_{2i}$  and

$\Gamma_{3i}$  using DE algorithm is conducted for searching the minimal sum of fundamental scattering energy within range  $\theta \in [-90^\circ, 90^\circ]$ . The corresponding target function and constraint conditions are shown in Eq. (11).

$$\begin{aligned} & \min_{0 < \Gamma_{1i}, \Gamma_{2i}, \Gamma_{3i} < 1} \int_{-\frac{\pi}{2}}^{\frac{\pi}{2}} f(\theta, t)_{m=0} d\theta \\ & s.t. \sum_{i=1}^{16} \Gamma_{2i} = 8, \quad \Gamma_{1i} + \Gamma_{2i} + \Gamma_{3i} = 1 \end{aligned} \tag{11}$$

Figure 3 shows the convergence process of duty ratios, where each iteration number is corresponding to 32 duty ratios in which “\*” represents  $\Gamma_{1i}$ , and “o” is for  $\Gamma_{2i}$ . Fig. 4 shows the switching waveforms of two AFSS layers. It is beneficial to minimize the fundamental scattering echo energy of PMS by using the waveforms in Fig. 4 to control active layers. It is found that  $\Gamma_{1i}$  and  $\Gamma_{2i}$  converge to 0.25 and 0.5, respectively. Therefore, the final optimal solution is  $\Gamma_{1i} = \Gamma_{3i} = 0.25$ ,  $\Gamma_{2i} = 0.5$ ,  $i = 1, 2 \dots 16$ . According to the definition of  $\Gamma_{ki}$ , the switching scheme of PMS is described as:

$$\tau_{1i}^{on} = (n - 1) T_p, \tau_{1i}^{off} = \tau_{2i}^{on} = 0.25nT_p, \tau_{2i}^{off} = \tau_{3i}^{on} = 0.75nT_p, \tau_{3i}^{off} = nT_p, i = 1, 2, 3 \dots 16 \tag{12}$$

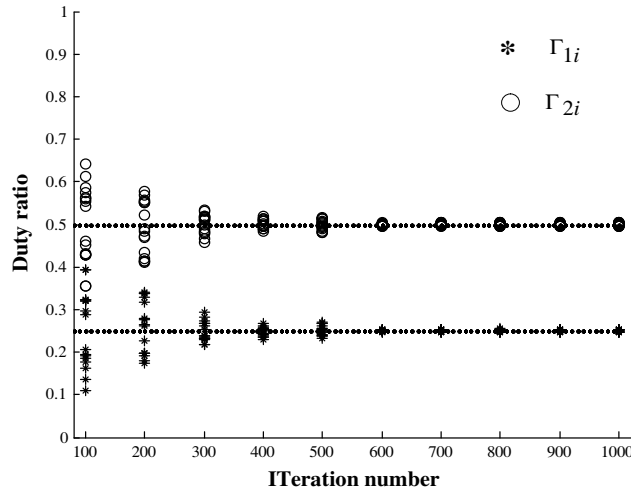


Figure 3. Iterative results of duty ratios.

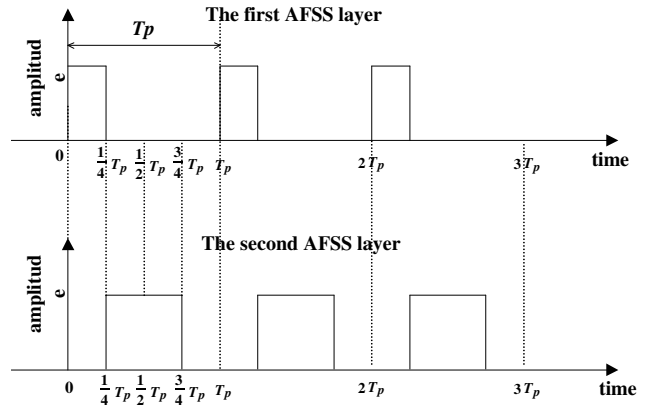


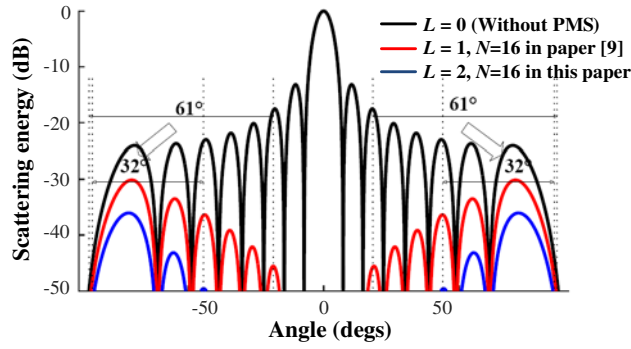
Figure 4. Switching waveforms of two AFSS layers.

#### 4. SIMULATION RESULTS

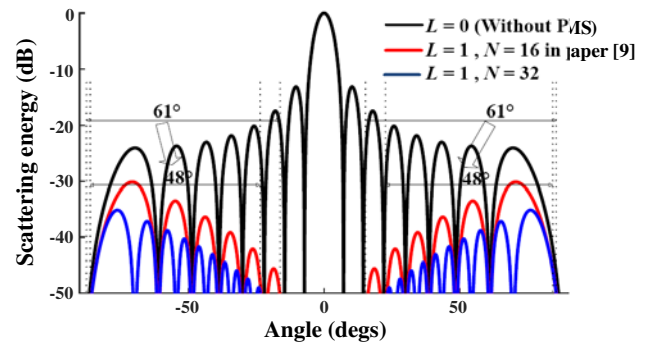
In order to compare with the single-active-layer PMS, we calculate the scattering pattern of two-active-layer PMS according to the analytical formulation (7) and the optimal solution in Eq. (12).

Figure 5 shows the angular scattering pattern at the fundamental frequency  $f_0$  when the number of AFSS layers  $L = 0, 1$  and  $2$ . We define  $E$  as the sum of scattering echo energy at  $f_0$ . It is found that  $E_{L=2} < E_{L=1} < E_{L=0}$ . We use  $\varphi$  to represent the sum of angle at which the scattering energy level is above  $-50$  dB to measure the spatial coverage of scattering echo energy. In the figure,  $\varphi$  is about 64 degrees when  $L = 2$ , which decreases by 58 degrees compared with the case  $\varphi$  equal to 122 degrees when  $L = 1$ . The scattering echo energy and its spatial coverage are both further reduced by adding one active layer.

The fundamental scattering energy of PMS is residue due to its finite size. So enlarging the size of PMS is also a method to improve the absorbing performance of PMS. Fig. 6 shows the angular scattering pattern at the fundamental frequency  $f_0$  with  $L = 1$  and  $N = 16$  or  $32$ . It is noted that PMS



**Figure 5.** Comparison diagram of the scattering energy at  $f_0$  when  $L = 0, 1$  and  $2$ .



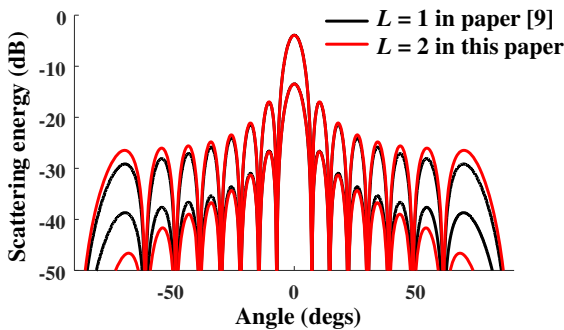
**Figure 6.** Comparison diagram of the scattering energy at  $f_0$  when  $N = 16$  and  $32$  ( $L = 1$ ).

with  $L = 1$  and  $N = 32$  has the same number of AFSS elements as the PMS with  $L = 2$  and  $N = 16$ . In Fig. 6, it is also found that  $E_{L=2} < E_{L=1} < E_{L=0}$ . However, the spatial coverage of scattering echo energy  $\varphi$  decreases from 122 degrees to only 96 degrees, and the decrement is smaller than the result of 58 degrees compared with PMS with  $L = 2$  and  $N = 16$ . Therefore, the method proposed in this paper has a better performance in improving the absorbing performance of PMS than enlarging the size of PMS directly.

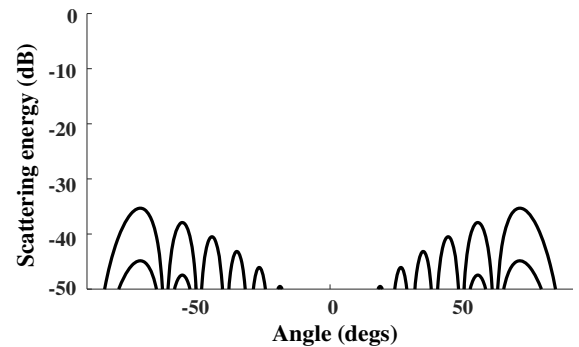
A further discussion is taken to explain the variation of  $E$ . The scattering energy of single-active-layer PMS is all zero at even harmonics [9]. However, from Eq. (7), only  $4n$ -harmonics are found zero in the case using two-active-layer PMS, which means that the 2nd, 6th ...  $(4n - 2)$ -harmonics are newly generated compared with the single-active-layer PMS. Fig. 7 shows the scattering energy at odd harmonics is almost invariant, the energy at  $(4n - 2)$ -harmonics probably comes from the incident frequency  $f_0$ , which explains the variation of  $E$  as  $L$  is from 1 to 2. Fig. 8 shows the scattering patterns at the first four even harmonics when  $L = 2$ . Only two curves which represents the 2nd and 6th harmonics are seen respectively in this figure. Fig. 9 shows the process of energy transformation in the spectrum. Because the fundamental scattering energy is redistributed to the newly generated harmonics partially, the former is reduced relatively as a result.

Figure 7 shows that the energy at the first harmonic is still high around the incident direction. Tennant and Chambers proved that the scattering energy at odd harmonics can be redistributed in the angular scattering pattern through anti-phase in some of the control waveforms in [9]. In this paper, a similar method is considered to reduce the scattering energy at odd harmonics around the incident direction.

We define sequence  $k_i = [X_i]_{i=1,2,3\dots 16}$ , where  $x_i = 1$  represents: within  $0 \sim 0.25T_p$ , the first



**Figure 7.** Comparison diagram of the scattering energy at the first two odd harmonics when  $L = 1$  and  $2$ .



**Figure 8.** Scattering energy at first four even harmonics when  $L = 2$ .

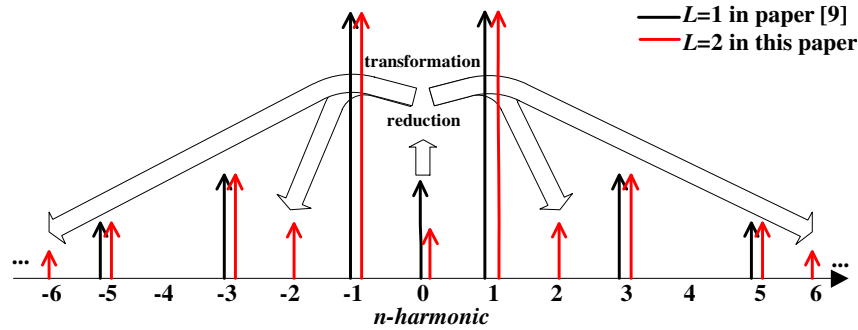


Figure 9. Schematic diagram of the scattering energy transfer in the spectrum.

AFSS layer is “on”;  $0.25T_p \sim 0.75T_p$ , the second AFSS layer is “on”;  $0.75T_p \sim T_p$ , both of them are “off”;  $x_i = 0$  represents: within  $0 \sim 0.25T_p$  and  $0.75T_p \sim T_p$ , the second AFSS layer is “on”;  $0.25T_p \sim 0.5T_p$ , the first AFSS layer is “on”;  $0.5T_p \sim 0.75T_p$ , both of them are “off”. Fig. 10 shows the corresponding control waveforms of 1 and 0. It is clear that the previous discussion is under the premise  $k_i = [1, 1, 1, 1, 1, 1, 1, 1, 1, 1, 1, 1, 1, 1, 1]$ .

As shown in Fig. 11, the scattering energy at the first harmonic and at the incident direction decreases continuously with the increasing number of 0 in  $k_i$ . Finally, this energy reaches zero when half the elements in  $k_i$  are 0. The sequence  $k'_i = [1, 0, 1, 0, 1, 0, 1, 0, 1, 0, 1, 0, 1, 0, 1, 0]$  is selected at last due to its excellent performance in reducing the harmonic scattering energy around the incident direction. The corresponding scattering pattern generated at odd harmonics is shown in Fig. 12. From the figure, the scattering energy around the incident direction has been reduced markedly compared with the case using  $k_i$ . This variation is meaningful when the working bandwidth of radar receiver is wide enough to cover the first harmonics.

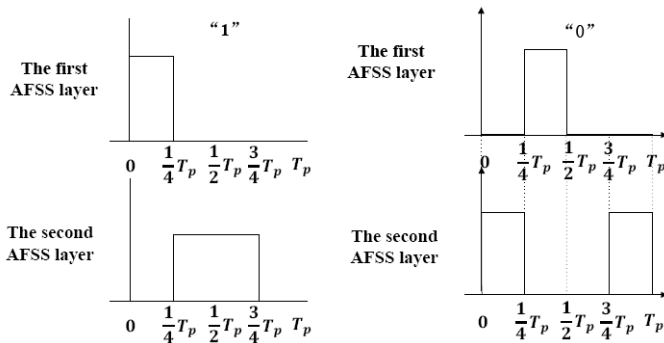


Figure 10. Control waveform of “1” and “0”.

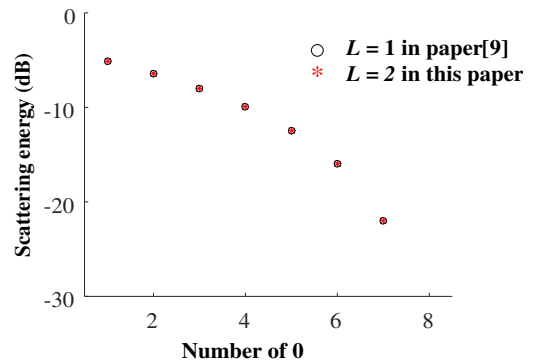
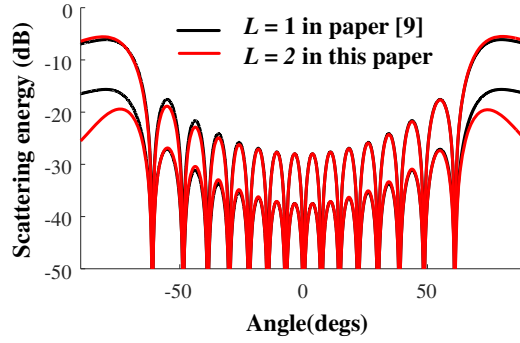


Figure 11. Variation of the scattering energy at the first harmonic and at the incident direction.

### 5. SUMMARY AND ANALYSIS

The discussion above indicates that PMS ( $L = 2$ ) has a better performance in reducing the scattering energy at the fundamental frequency than PMS ( $L = 1$ ). In this section, we increase the value of  $L$  to research the scattering properties of multi-active-layer PMS.

Considering the case  $L = 3$ , duty ratios of the control waveforms are optimized similarly as in Section 3, and the convergence results are  $\Gamma_{1i} = \Gamma_{4i} = 1/8$ ,  $\Gamma_{2i} = \Gamma_{3i} = 3/8$ ,  $i = 1, 2 \dots 16$ . Fig. 13 indicates that the fundamental scattering energy  $E$  and its spatial coverage  $\varphi$  are both further reduced compared with the case  $L = 2$ , where it is reduced from approximately 64 degrees to 36 degrees. To



**Figure 12.** Comparison diagram of the scattering energy at the first two odd harmonics when  $L = 1$  and 2 ( $k'_i = [1, 0, 1, 0, 1, 0, 1, 0, 1, 0, 1, 0, 1, 0]$ ).

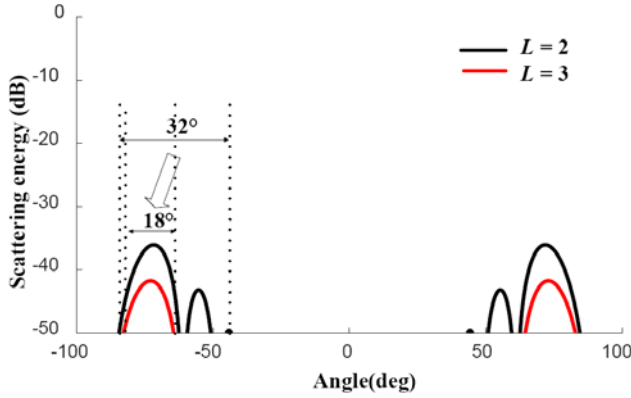


**Figure 13.** Comparison diagram of the scattering energy at  $f_0$  when  $L = 2$  and 3.

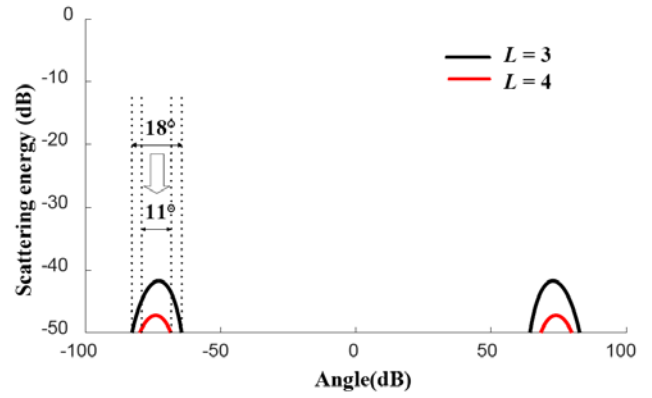


**Figure 14.** Comparison diagram of the scattering energy at  $f_0$  when  $L = 3$  and 4.

explain this variation, the scattering energy is zero at  $8n$ -harmonics when  $L = 3$ . In other words, more energy is transformed from fundamental frequency to  $(8n - 4)$ -harmonics. However, it is noted that the reduction in  $\varphi$  is 28 degrees in this case, which is smaller than the result of 58 degrees when  $L$  changes from 1 to 2.

As the same way for the case  $L = 4$ , the optimized duty ratios are  $\Gamma_{1i} = \Gamma_{5i} = 1/16$ ,  $\Gamma_{2i} = \Gamma_{4i} = 1/4$ ,  $\Gamma_{3i} = 3/8$ ,  $i = 1, 2 \dots 16$ . The scattering pattern is shown in Fig. 14 and is reduced from approximately 36 degrees to 22 degrees. The decreasing trend is continuous, but the falling range, 14 degrees, is even smaller than the previous result 28 degrees.

A summary on the mathematical relationship between duty ratios of the control waveforms and  $L$  is given in Eq. (14), which indicates that the duty ratio follows the binomial distribution. On this precondition, fundamental scattering energy and its spatial coverage always reaches the minimum under specific value of  $L$ .

$$\Gamma_{ki} = \frac{C_m^{k-1}}{2^m}, \quad k = 1, 2, 3 \dots m + 1 \quad (13)$$

According to the above discussion, the reductions in  $E$  and  $\varphi$  are both further enhanced as the value of  $L$  increases. We define  $Q = E \cdot \varphi$  to measure the influence degree of fundamental scattering energy. Fig. 15 gives its variation tendency as  $L$  increases. A marked reduction in  $Q$  occurs as  $L$  changes from 1 to 2 and 2 to 3, but an almost invariant process is seen after  $L = 3$ . This floor effort limits the increasing value of  $L$ . Therefore, PMS with  $L = 2$  or 3 is beneficial for balancing the scattering performance and structure complexity.

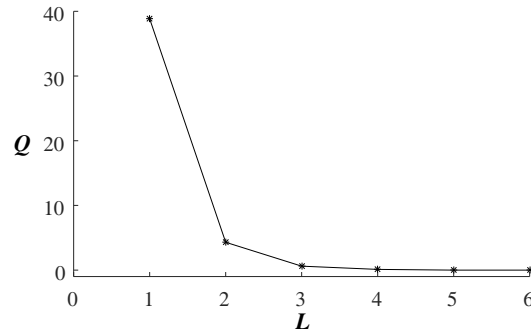


**Figure 15.** Variation in  $Q$  as  $L$  increases.

## 6. CONCLUSION

In this paper, we study the scattering properties of multi-active-layer PMS. DE algorithm is employed for optimizing the switching scheme of PMS. The optimized switching scheme is confirmed meaningful in reducing the spatial coverage of scattering echo at incident frequency. A conclusion on the number of active layers used in the PMS is drawn after balancing the scattering performance and the structure complexity of PMS. A further research applies PMS to the directional modulation (DM) communication system.

## ACKNOWLEDGMENT

This research was supported by the National Nature Foundation of China (Grant No. 61302102, No. 61271232) and the Natural Science Foundation of Jiangsu Provincial College (Grant No. 13KJB510023), all support is gratefully acknowledged.

## REFERENCES

1. Nair, R. U. and R. M. Jha, "Broadbanding of A-sandwich radome using Jerusalem cross frequency selective surface," *CMC: Computers, Materials & Continua*, Vol. 37, No. 2, 109–121, 2013.
2. Sazegar, M., Y. Zheng, C. Kohler, et al., "Beam steering transmitarray using tunable frequency selective surface with integrated ferroelectric varactors," *IEEE Transactions on Antennas and Propagation*, Vol. 60, No. 12, 5690–5699, 2012.
3. Wu, P., F. Bai, Q. Xue, et al., "Use of frequency-selective surface for suppressing radio-frequency interference from wireless charging pads," *IEEE Transactions on Industrial Electronics*, Vol. 61, No. 8, 3969–3977, 2014.
4. Tennant, A. and B. Chambers, "A single-layer tunable microwave absorber using an active FSS," *IEEE Microwave and Wireless Components Letters*, Vol. 14, No. 1, 46–47, 2004.
5. Chambers, B. and A. Tennant, "The phase-switched screen," *IEEE Antennas and Propagation Magazine*, Vol. 46, No. 6, 23–37, 2004.
6. Chambers, B. and A. Tennant, "A smart radar absorber based on the phase-switched screen," *IEEE Transactions on Antennas and Propagation*, Vol. 53, No. 1, 394–403, 2005.
7. Tennant, A. and B. Chambers, "Experimental performance of a phase-switched screen against modulated microwave signals," *IEE Proceedings-Radar, Sonar and Navigation*, Vol. 152, No. 1, 29–33, 2005.
8. Chambers, B. and A. Tennant, "FDTD modelling of active radar absorbers," *IEEE Antennas and Propagation Society International Symposium*, 6027–6030, 2007.
9. Tennant, A. and B. Chambers, "Time-switched array analysis of phase-switched screens," *IEEE Transactions on Antennas and Propagation*, Vol. 57, No. 3, 808–812, 2009.

10. Chambers, B. and A. Tennant, "Reflectivity null tuning in multi-layer phase-switched active radar absorbers," *IEE Proceedings-Radar, Sonar and Navigation*, Vol. 152, No. 4, 245–247, 2005.
11. Tennant, A. and B. Chambers, "Experimental two-layer adaptive phase-switched screen," *Electronics Letters*, Vol. 37, No. 23, 1379–1380, 2001.
12. Xu, W., Y. He, P. Kong, et al., "An ultra-thin broadband active frequency selective surface absorber for ultrahigh-frequency applications," *Journal of Applied Physics*, Vol. 118, No. 18, 184903, 2015.
13. Tennant, A. and B. Chambers, "RCS reduction of spiral patch antenna using a PSS boundary," *IEE Proceedings-Radar, Sonar and Navigation*, Vol. 152, No. 4, 248–252, 2005.
14. Tennant, A. and B. Chambers, "SSB-type frequency scattering from a single-layer PSS with interlaced element modulation," *IEEE Antennas and Wireless Propagation Letters*, Vol. 5, No. 1, 284–285, 2006.
15. Tennant, A. and B. Chambers, "In-phase and quadrature modulated scatterer," *Electronics Letters*, Vol. 38, No. 11, 498–499, 2002.
16. Chambers, B., A. Tennant, and A. Melnikov, "Detection of a radar signal reflected from a phase-modulated surface," *IEE Proceedings-Radar, Sonar and Navigation*, Vol. 153, No. 4, 316–324, 2006.
17. Balci, O., E. O. Polat, N. Kakenov, et al., "Graphene-enabled electrically switchable radar-absorbing surfaces," *Nature Communications*, Vol. 6, 6628–6628, 2014.
18. Zabri, S. N., R. Cahill, G. Conway, et al., "Inkjet printing of resistively loaded FSS for microwave absorbers," *Electronics Letters*, Vol. 51, No. 13, 999–1001, 2015.
19. Xia, T., Y. Cao, N. A. Oyler, et al., "Strong microwave absorption of hydrogenated wide bandgap semiconductor nanoparticles," *ACS Applied Materials & Interfaces*, Vol. 7, No. 19, 10407–10413, 2015.